PERGAMON

International Journal of Solids and Structures 38 (2001) 4937–4954

INTERNATIONAL JOURNAL OF SOLIDS and STRUCTURES

www.elsevier.com/locate/ijsolstr

A semi-analytical solution for vibration of rectangular plates with abrupt thickness variation ☆

K.M. Liew [a,*], T.Y. Ng [b], S. Kitipornchai [c]

[a] *Centre for Advanced Numerical Engineering Simulations, School of Mechanical and Production Engineering, Nanyang Technological University, Nanyang Avenue, Singapore 639798*

[b] *Institute of High Performance Computing, National University of Singapore, 89C Science Park Drive, #02-11/12, The Rutherford, Singapore Science Park 1, Singapore 118261*

[c] *Department of Civil Engineering, University of Queensland, Brisbane, Qld 4072, Australia*

Received 18 February 2000

Abstract

A semi-analytical analysis of free vibration of plates with cross-sectional discontinuities due to abrupt changes in thickness is presented. A basic square element divided into suitable subdomains dependent upon the positions of these abrupt changes is used as the basic building element. Admissible functions that satisfy the essential or geometric boundary conditions are used to define the transverse deflection of each subdomain. Continuities in the displacement, slope, moment and higher derivatives between adjacent subdomains are enforced at the interconnecting edges. The resulting global energy functional from the proper assembly of the coupled strain and kinetic energy contributions of each subdomain is then minimized via the Ritz procedure to extract the frequencies and mode shapes. Contour plots of a range of new mode shapes are presented for the enhancement of understanding the dynamic behavior of this class of plates.

Keywords: Abrupt thickness variation; Free vibration; Plates; Polynomials; Ritz method

1. Introduction

Thin plate elements have found application in most branches of engineering and the study of this basic structural member is of immense practical interest in marine, aeronautical, civil, mechanical and naval engineering design. This paper examines the vibration characteristics of thin isotropic plates with cross sectional discontinuities due to abrupt changes in thickness. Plates with these discontinuities are often encountered in printed circuit board designs. These abrupt changes in thickness are present usually to improve heat transfer characteristics as well as to fulfil certain assembly and packaging requirements. Due

☆ This work was partially supported by Singapore-MIT Alliance – Program for High Performance Computation for Engineering Systems.

* Corresponding author. Tel.: +65-790-4076; fax: +65-791-1859/+65-793-6763.
E-mail address: mkmliew@ntu.edu.sg (K.M. Liew).

0020-7683/01/$ - see front matter
PII: S0020-7683(00)00329-2

to the complicating effects of the abrupt thickness variation, conventional continuum methods cannot be directly applied. With the implementation of some form of discretization and proper enforcement of resulting continuity requirements, however, continuum methods such as the Ritz method can be applied with a great measure of success.

Discrete methods have been most popular for analyzing plates with abrupt changes in thickness as well as cutouts. Of the various discrete methods available, the finite element method (FEM) is by far the most widely used method for this class of problems. Notable recent works are Boay (1996), Sabir and Davies (1997) and Sivakumar et al. (1999a,b). The boundary element method, though considerably less often used for these problems compared to the FEM, has also been successfully employed to analyze plates with irregularities such as cracks and holes. Published works include Pan (1997) and Chau and Wang (1999). A more recent development for the solution of plates with discontinuities is the differential quadrature element method which was successfully used by Liu and Liew (1999a,b) for the vibration analysis of discontinuous Mindlin plates.

Although discrete methods have been proven reliable for solving the presently defined problem, the major drawback is that they are in general very computationally intensive with substantial demands on data storage space and CPU time. Semi-analytical solution methods thus provide a very attractive alternative. Prominent works include the semi-analytical isoparametric strip distributed transfer function method which was developed and successfully used by Yang and Zhou (1996) and Yang and Park (1999) for the analysis of irregularly shaped plates and plates with curved boundaries. Geannakakes (1990) also presented a semi-analytical finite strip method utilizing beam characteristic orthogonal polynomials for the vibration analysis of arbitrarily shaped plates. An efficient and accurate semi-analytical method based on the Rayleigh–Ritz procedure by using characteristic beam functions was developed by Lam et al. (1989) for the analysis of rectangular plates with cutouts and material non-homogeneity. Further works based on semi-analytical methods were presented by Laura et al. (1990, 1997) via an optimized Rayleigh–Ritz method for the vibration of plates with thickness discontinuities.

The present work develops and utilizes the highly efficient and elegant domain decomposition method, which is essentially a semi-analytical approach with discretization occurring only along the lines adjoining major rectangular subdomains. This approach has been successfully employed for the treatments of various mixed-edge boundary conditions and sharp re-entrant geometries in plate analyses, see Liew et al. (1993a,b, 1995) and Liew and Sum (1998). This semi-analytical method is now proposed for the treatment of plates with cross sectional discontinuities or, more specifically, abrupt changes in the thickness. Through the use of the domain decomposition method, a complex plate configuration is decomposed into appropriate subdomains and orthogonally generated admissible polynomials are used as displacement functions. Sets of continuity matrices are then computed from the compatibility conditions at the interconnecting edges so as to couple the eigenvectors of adjoining subdomains. The global energy functional is obtained by the proper assembly of the individual stiffness and mass matrices of each subdomain and the Ritz procedure is then employed to extract the natural frequencies. Where possible, verification of the present formulation is provided via comparison with results from open literature. Further, a range of new mode shapes is presented for various boundary condition types.

2. Theoretical formulation

2.1. Basic building block and notation

The basic building block employed here is of square domain as shown in Fig. 1. The plate is assumed to be thin, isotropic and homogeneous in all subdomains so that the Kirchoff–Love plate theory is applicable. In Fig. 1, a/b is the aspect ratio and γ is the geometric ratio. Subdomains 1–3 have similar flexural ri-

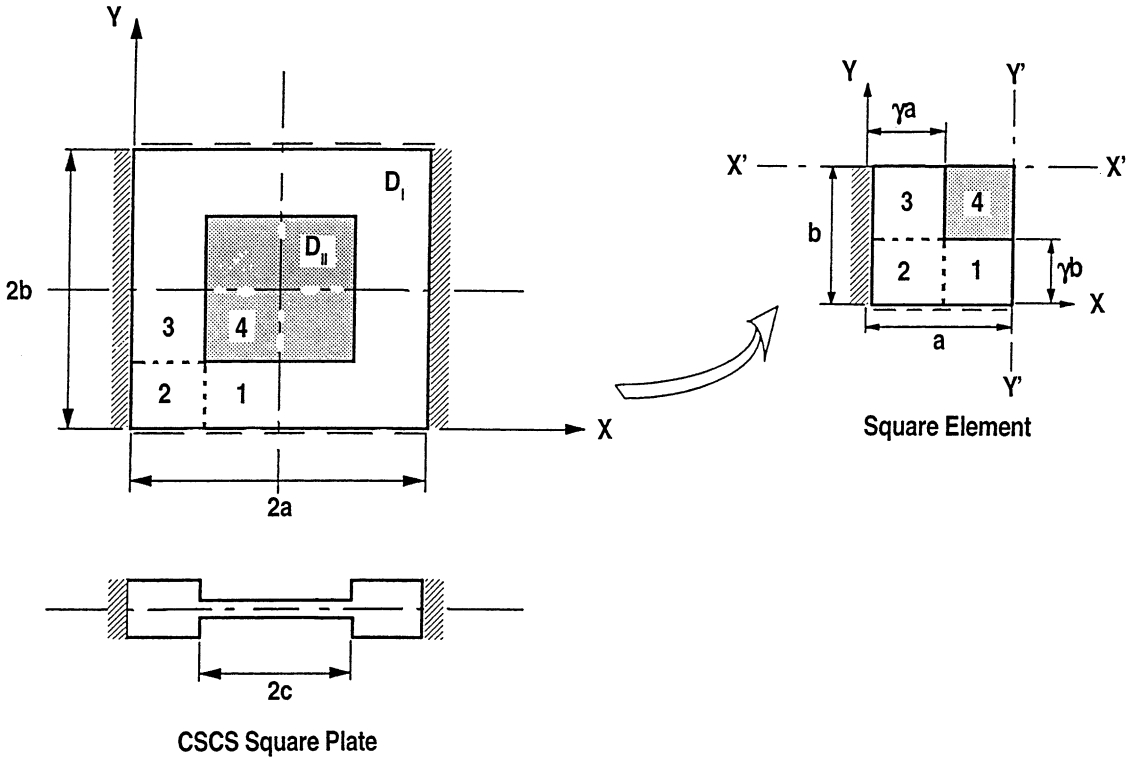

Fig. 1. Geometry definition of a CSCS square plate with internal discontinuity.

gidities, $D_{\mathrm{I}} = 4D$, while subdomain 4 has a flexural rigidity of $D_{\mathrm{II}} = D$. Thus the mass matrices of subdomains 1–3 can be pre-multiplied by a factor of $\sqrt[3]{4.0}$ prior to assembly so as to account for the variation in the thickness. In the subsequent derivation, the superscript $\{\varepsilon\}$ denotes the subdomain indices with $\varepsilon = 1$, 2, 3 and 4. A very small Poisson's ratio is assumed for the purpose of comparison with results reported by Lam et al. (1989).

In the present study, a square plate is assumed. Three types of boundary conditions have been considered, namely: the simply supported case, the clamped–simply supported–clamped-simply supported (CSCS) case and the fully clamped case. For all three cases, the edge ratio for the discontinuity is given by $c/a = 0.4$.

2.2. Polynomial based displacement functions

To apply the Ritz method, the plate domain is sub-divided into smaller rectangular subdomains as shown in Fig. 1. At each subdomain, a set of piecewise continuous displacement functions is assumed. These functions are chosen so that they satisfy the essential geometric boundary conditions of each subdomain. The general forms of these displacement functions are

$$W^{\{\varepsilon\}}(x,y) = \sum_{i=1}^{I}\sum_{j=1}^{J} C_{ij}^{\{\varepsilon\}} \phi_i(x)^{\{\varepsilon\}} \psi_j(y)^{\{\varepsilon\}} \tag{1}$$

where $\phi_i(x)$ and $\psi_j(y)$ are the admissible trial functions in the x and y directions respectively; and $\varepsilon = \{1, 2, 3, 4\}$ represents the subdomain index. Depending on the relative location of each subdomain, the respective

displacement function shares an identically generated set of admissible functions either in the x or y direction, i.e.

$$\phi_i(x)^{\{\varepsilon_1\}} = \phi_i(x)^{\{\varepsilon_2\}}; \quad i = 1,2,3,\ldots,I; \qquad \{\varepsilon_1,\varepsilon_2\} \in \varepsilon \tag{2a}$$

$$\psi_j(y)^{\{\varepsilon_1\}} = \psi_j(y)^{\{\varepsilon_2\}}; \quad j = 1,2,3,\ldots,J; \qquad \{\varepsilon_1,\varepsilon_2\} \in \varepsilon \tag{2b}$$

The admissible functions $\phi_i(x)$ and $\psi_j(y)$ are sets of characteristic orthogonal polynomial functions generated by the Gram–Schmidt orthogonalization process (Chihara, 1978). These functions are essentially the product of a basic function and an orthogonal polynomial space. The basic functions $\phi_i(x)$ and $\psi_j(y)$ are chosen to satisfy at least the geometric boundary conditions of the subdomain and may be expressed as follows:

$$\phi_1(x) = \prod_{i=1}^{2}[\Gamma_i(x)]^{\Omega_i} \tag{3a}$$

$$\psi_1(y) = \prod_{i=1}^{2}[\Gamma_i(y)]^{\Omega_i} \tag{3b}$$

where the Γ_is are the boundary equations of the ith supporting edge and the Ω_is take the following forms

$$\Omega_i = 0 \quad \text{if the } i\text{th edge is free} \tag{4a}$$

$$\Omega_i = 1 \quad \text{if the } i\text{th edge is simply supported} \tag{4b}$$

$$\Omega_i = 2 \quad \text{if the } i\text{th edge is clamped} \tag{4c}$$

The higher order polynomial terms are generated using the Gram–Schmidt orthogonalization process

$$\phi_{k+1}(x) = \{g(x) - \Xi_k^A\}\phi_k(x) - \Xi_k^B\phi_{k-1}(x); \quad k = 1,2,3\ldots \tag{5}$$

where

$$\Xi_k^A = \frac{{}_1\Delta_k}{{}_2\Delta_k}; \qquad \Xi_k^B = \frac{{}_2\Delta_k}{{}_3\Delta_{k-1}} \tag{6a}$$

$${}_1\Delta_k = \int_0^a g(x)\phi_k^2(x)\,\mathrm{d}x \tag{6b}$$

$${}_2\Delta_k = \int_0^a \phi_k^2(x)\,\mathrm{d}x \tag{6c}$$

$${}_3\Delta_{k-1} = \int_0^a \phi_{k-1}^2(x)\,\mathrm{d}x \tag{6d}$$

where $g(x)$ is an arbitrary function chosen to ensure that the higher order orthogonal functions satisfy the geometric boundary conditions. The polynomial $\phi_0(x)$ is defined as zero and the set of polynomials generated satisfies the orthogonality condition

$$\int_0^a \phi_i(x)\phi_j(x)\,\mathrm{d}x = \delta_{ij}; \quad i,j = 1,2,3\ldots \tag{7}$$

where δ_{ij} is the Kronecker delta. The orthogonal functions in the y direction can be generated in similar fashion where the limits of integration now range from 0 to b.

2.3. Continuity consideration

To satisfy the compatibility requirement at the interconnecting boundaries, the continuities in deflection, slope and higher derivatives are enforced concurrently at evenly distributed quadrature segments along the boundaries. The method of subdomain weighted residual (Grandin, 1986), is subsequently applied at these quadrature segments

$$\int_{s_i} E(s)\vartheta(s)\,\mathrm{d}s = 0; \quad i = 1,2,3,\ldots,Mq \tag{8}$$

with a weighting function $\vartheta(s)$ of unity. In Eq. (8), $E(s)$ is the error function representing the relative difference in displacement, slope and higher derivatives between adjacent subdomains. This function is minimized simultaneously over separate regions of the integral. In explicit forms, this implies

$$\int_{s_{n-1}}^{s_n} \mathbf{N}\left(W^{\{\varepsilon\}} - W^{\{\varepsilon-1\}}\right)\mathrm{d}s = 0 \tag{9a}$$

where $\mathbf{N}$ denotes the matrix containing the respective differential operators

$$\mathbf{N} = \left[\,1 \quad \tfrac{\partial}{\partial s} \quad \cdots \quad \tfrac{\partial^r}{\partial s^r}\,\right]^{\mathrm{T}}_{r\times 1} \tag{9b}$$

with $n = 1, 2, 3,\ldots Mq$; $\varepsilon = 1, 2, 3, 4$; $r = 1, 2, 3,\ldots, J-1$; and $s = x$ or y depending on the direction of the continuities to be enforced. The deflection functions, $W(x,y)$, of each subdomain have been defined in Eq. (1). A set of continuity matrices that couple the eigenvectors, C_{ij}, of the adjacent subdomains can be obtained directly from the above simultaneous equations. This process is illustrated for subdomains 1 and 2. In Fig. 1, it can be seen that the two subdomains share an identical set of admissible functions in the x direction

$$\phi_i(x)^{\{1\}} = \phi_i(x)^{\{2\}}; \quad i = 1,2,\ldots,I \tag{10}$$

From Eqs. (9a), (9b) and (10), the following set of simultaneous equations is obtained:

$$\mathbf{G}\cdot\mathbf{R} = 0 \tag{11a}$$

$$\mathbf{G} = \begin{bmatrix} \phi_1(x)^{(1)} & \phi_2(x)^{(1)} & \cdots & \phi_i(x)^{(1)} & \cdots & \phi_I(x)^{(1)} \\ \frac{\partial\phi_1(x)^{(1)}}{\partial x} & \frac{\partial\phi_2(x)^{(1)}}{\partial x} & \cdots & \frac{\partial\phi_i(x)^{(1)}}{\partial x} & \cdots & \frac{\partial\phi_I(x)^{(1)}}{\partial x} \\ \vdots & \vdots & & \vdots & & \vdots \\ \frac{\partial^i\phi_1(x)^{(1)}}{\partial x^i} & \frac{\partial^i\phi_2(x)^{(1)}}{\partial x^i} & \cdots & \frac{\partial^i\phi_i(x)^{(1)}}{\partial x^i} & \cdots & \frac{\partial^i\phi_I(x)^{(1)}}{\partial x^i} \\ \vdots & \vdots & & \vdots & & \vdots \\ \frac{\partial^r\phi_1(x)^{(1)}}{\partial x^r} & \frac{\partial^r\phi_2(x)^{(1)}}{\partial x^r} & \cdots & \frac{\partial^r\phi_i(x)^{(1)}}{\partial x^r} & \cdots & \frac{\partial^r\phi_I(x)^{(1)}}{\partial x^r} \end{bmatrix} \tag{11b}$$

$$\mathbf{R} = \left[\,\Re_1 \quad \Re_2 \quad \cdots \quad \Re_i \quad \cdots \quad \Re_I\,\right] \tag{11c}$$

where $r = 1, 2, 3,\ldots$; and

$$\Re_i = \left[\sum_{j=1}^{J} C_{ij}^{\{1\}} \int \psi_j(y)^{\{1\}}\,\mathrm{d}y - \sum_{j=1}^{J} C_{ij}^{\{2\}} \int \psi_j(y)^{\{2\}}\,\mathrm{d}y\right] \tag{12}$$

The integration in Eq. (12) is performed over the respective quadrature segments distributed along the interconnecting boundary. To satisfy Eq. (11a)–(11c) simultaneously, all the terms in $\Re_i$ must vanish identically

$$\mathfrak{R}_1 = \mathfrak{R}_2 = \mathfrak{R}_3 = \cdots = \mathfrak{R}_I = 0 \tag{13}$$

From Eq. (13), the continuity matrix that couple the eigenvectors of subdomains 1 and 2 is obtained

$$\left\{C^{\{2\}}\right\} = \left[P^{\{2\}}\right]\left\{C^{\{1\}}\right\} \tag{14}$$

where

$$\left[P^{\{2\}}\right] = \begin{bmatrix} [p] & & & \\ & [p] & & \\ & & \ddots & \\ & & & [p] \end{bmatrix} \tag{15}$$

in which

$$[p] = \left[q^{\{2\}}\right]^{+}\left[q^{\{1\}}\right] \tag{16}$$

where $\left[q^{\{\varepsilon\}}\right]^{+}$ is the generalized inverse of a fully populated matrix $[q^{\{\varepsilon\}}]$ of the form

$$\left[q^{\{\varepsilon\}}\right] = \begin{bmatrix} q_{11}^{\{\varepsilon\}} & q_{12}^{\{\varepsilon\}} & q_{13}^{\{\varepsilon\}} & \cdots & q_{1j}^{\{\varepsilon\}} & \cdots & q_{1J}^{\{\varepsilon\}} \\ q_{21}^{\{\varepsilon\}} & q_{22}^{\{\varepsilon\}} & q_{23}^{\{\varepsilon\}} & \cdots & q_{2j}^{\{\varepsilon\}} & \cdots & q_{2J}^{\{\varepsilon\}} \\ \vdots & \vdots & \vdots & & \vdots & & \vdots \\ q_{n1}^{\{\varepsilon\}} & q_{n2}^{\{\varepsilon\}} & q_{n3}^{\{\varepsilon\}} & \cdots & q_{nj}^{\{\varepsilon\}} & \cdots & q_{nJ}^{\{\varepsilon\}} \\ \vdots & \vdots & \vdots & & \vdots & & \vdots \\ q_{Mq1}^{\{\varepsilon\}} & q_{Mq2}^{\{\varepsilon\}} & q_{Mq3}^{\{\varepsilon\}} & \cdots & q_{Mqj}^{\{\varepsilon\}} & \cdots & q_{MqJ}^{\{\varepsilon\}} \end{bmatrix} \tag{17}$$

The generalized inverse $\left[q^{\{\varepsilon\}}\right]^{+}$ is derived from the singular-value decomposition of $\left[q^{\{\varepsilon\}}\right]$ via the Rao and Mitra (1971) generalized inversion procedure

$$\left[q^{\{\varepsilon\}}\right]^{+} = \left(\left[q^{\{\varepsilon\}}\right]^{\mathrm{H}}\left[q^{\{\varepsilon\}}\right]\right)^{-1}\left[q^{\{\varepsilon\}}\right]^{\mathrm{H}} \tag{18}$$

where $\left[q^{\{\varepsilon\}}\right]^{\mathrm{H}}$ is the Hermitian transpose of $\left[q^{\{\varepsilon\}}\right]$. The element of the matrix, $q_{nj}^{\{\varepsilon\}}$, are computed from the following integrations:

$$q_{ni}^{\{\varepsilon\}} = \int_{x_{n-1}}^{x_n} \phi_i(x)^{\{\varepsilon\}}\mathrm{d}x \tag{19a}$$

$$q_{nj}^{\{\varepsilon\}} = \int_{y_{n-1}}^{y_n} \psi_j(y)^{\{\varepsilon\}}\mathrm{d}y \tag{19b}$$

The subscript n in the above expression represents the indices of the quadrature segments whereas the subscripts i and j represent the indices of the polynomial functions. The derivation of the continuity matrix described above can be easily generalized to three or more subdomains and in this case as shown in Fig. 1, there are four subdomains under consideration.

2.4. Global energy functional

The maximum strain and kinetic energies for a given rectangular element with small deflection vibration are given by

$$U_{\max}^{\{\varepsilon\}} = \frac{D}{2}\int\int_A (W_{xx}^2 + 2vW_{xx}W_{yy} + W_{yy}^2 + 2(1-v)W_{xy}^2)\,\mathrm{d}A, \tag{20}$$

$$T_{\max}^{\{\varepsilon\}} = \frac{\rho h\omega^2}{2}\int\int_A W^2\,\mathrm{d}A \tag{21}$$

where the subscripts x and y denote partial derivatives with respect to x and y respectively. The natural frequency is denoted by ω. The strain energy, $U^{\{\varepsilon\}}$, and kinetic energy, $T^{\{\varepsilon\}}$, for a rectangular subdomain, $\{\varepsilon\}$, can be expressed in terms of the eigenvectors, C_{ij}, of the nth subdomain

$$U^{\{\varepsilon\}} = \frac{1}{2}\int_A \left\{C^{\{1\}}\right\}^{\mathrm{T}}\left[\bar{K}^{\{\varepsilon\}}\right]\left\{C^{\{1\}}\right\}\mathrm{d}A \tag{22}$$

$$T^{\{\varepsilon\}} = \frac{1}{2}\int_A \left\{C^{\{1\}}\right\}^{\mathrm{T}}\left[\bar{M}^{\{\varepsilon\}}\right]\left\{C^{\{1\}}\right\}\mathrm{d}A \tag{23}$$

The transformed stiffness matrix $\left[\bar{K}^{\{\varepsilon\}}\right]$ and mass matrix $\left[\bar{M}^{\{\varepsilon\}}\right]$ for subdomain $\{\varepsilon\}$ are derived from the continuity matrix $\left[P^{\{\varepsilon\}}\right]$ of Eq. (15) which is related to the matrix $\left[Q^{\{\varepsilon\}}\right]$ by Eq. (26) in the following manner:

$$[\bar{K}^{\{\varepsilon\}}] = [Q^{\{\varepsilon\}}]^{\mathrm{T}}[K^{\{\varepsilon\}}][Q^{\{\varepsilon\}}] \tag{24}$$

$$[\bar{M}^{\{\varepsilon\}}] = [Q^{\{\varepsilon\}}]^{\mathrm{T}}[M^{\{\varepsilon\}}][Q^{\{\varepsilon\}}] \tag{25}$$

$$[Q^{\{\varepsilon\}}] = \prod_{s=2}^{\varepsilon}[P^{\{s\}}] \tag{26}$$

For an isotropic plate, the stiffness matrix is expressed as

$$[\mathbf{K}] = [\mathbf{E}]^{\mathrm{T}}[\mathbf{F}] \tag{27}$$

$$[\mathbf{E}] = \begin{bmatrix} E^{2,2} \\ E^{0,0} \\ vE^{0,2} \\ vE^{2,0} \\ 2(1-v)E^{1,1} \end{bmatrix}_{5\times I^2}, \qquad [\mathbf{F}] = \begin{bmatrix} F^{0,0} \\ F^{2,2} \\ F^{2,0} \\ F^{0,2} \\ F^{1,1} \end{bmatrix}_{5\times J^2} \tag{28a, b}$$

$$[E^{r,s}]_{1\times I^2} = [E_{11}^{r,s}\ \ E_{12}^{r,s}\ \ \cdots\ \ E_{1I}^{r,s}\ \ E_{21}^{r,s}\ \ E_{22}^{r,s}\ \ \cdots\ \ E_{2I}^{r,s}\ \ \cdots\ \ E_{i1}^{r,s}\ \ E_{i2}^{r,s}\ \ \cdots\ \ E_{iI}^{r,s}\ \ \cdots\ \ E_{I1}^{r,s}\ \ E_{I2}^{r,s}\ \ \cdots\ \ E_{II}^{r,s}] \tag{29a}$$

$$[F^{r,s}]_{1\times J^2} = [F_{11}^{r,s}\ \ F_{12}^{r,s}\ \ \cdots\ \ F_{1I}^{r,s}\ \ F_{21}^{r,s}\ \ F_{22}^{r,s}\ \ \cdots\ \ F_{2I}^{r,s}\ \ \cdots\ \ F_{i1}^{r,s}\ \ F_{i2}^{r,s}\ \ \cdots\ \ F_{iI}^{r,s}\ \ \cdots\ \ F_{I1}^{r,s}\ \ F_{I2}^{r,s}\ \ \cdots\ \ F_{II}^{r,s}] \tag{29b}$$

$$E_{ij}^{r,s} = \int_0^a \left[\frac{\mathrm{d}^r\phi_i}{\mathrm{d}x^r}\frac{\mathrm{d}^s\phi_j}{\mathrm{d}x^s}\right]\mathrm{d}x \tag{30a}$$

$$F_{ij}^{r,s} = \int_0^b \left[\frac{\mathrm{d}^r\psi_i}{\mathrm{d}y^r}\frac{\mathrm{d}^s\psi_j}{\mathrm{d}y^s}\right]\mathrm{d}y \tag{30b}$$

in which $r, s = 0, 1, 2$. The limits of integration in Eqs. (30a) and (30b) depend on the x and y dimensions of the individual subdomain. The mass matrix is expressed as

$$[\mathbf{M}]_{I^2\times J^2} = \left[E^{0,0}\right]^{\mathrm{T}}\left[F^{0,0}\right] \tag{31}$$

The respective strain and kinetic energies of each subdomain are assembled to form the global strain energy, $\boldsymbol{U}$, and kinetic energy, $\boldsymbol{K}$, of the entire square plate domain as the sum of the contribution from each subdomain

$$\boldsymbol{U} = \sum_{\varepsilon=1}^{4} U^{\{\varepsilon\}} \tag{32a}$$

$$\boldsymbol{K} = \sum_{\varepsilon=1}^{4} T^{\{\varepsilon\}} \tag{32b}$$

Substituting the global strain energy and kinetic energy into the total energy functional

$$\boldsymbol{F} = \boldsymbol{U} - \boldsymbol{T} \tag{33}$$

and applying the Ritz minimization

$$\frac{\partial \boldsymbol{F}}{\partial C_{ij}^{\{1\}}} = 0; \quad i,j = 1,2,3,\ldots \tag{34}$$

leads to the governing eigenvalue equation for the entire plate

$$([\boldsymbol{K}_{\mathrm{T}}] - \omega^2[\boldsymbol{M}_{\mathrm{T}}])\{C^{\{1\}}\} = \{0\} \tag{35}$$

The elements of the global stiffness matrix, $[\boldsymbol{K}_{\mathrm{T}}]$, and the global mass matrix, $[\boldsymbol{M}_{\mathrm{T}}]$, are given by

$$[\boldsymbol{K}_{\mathrm{T}}] = \sum_{\varepsilon=1}^{4} [\bar{K}^{\{\varepsilon\}}] \tag{36}$$

$$[\boldsymbol{M}_{\mathrm{T}}] = \sum_{\varepsilon=1}^{4} [\bar{M}^{\{\varepsilon\}}] \tag{37}$$

The natural frequencies and mode shapes are obtained by solving this resulting governing eigenvalue equation. The eigenvalues are expressed in terms of a non-dimensional frequency parameter, λ, given by

$$\lambda = \omega a^2 \sqrt{\frac{\rho h}{D}} \tag{38}$$

The merit of the present method based on the above formulation is that regardless of the number of subdomains, the assembly process of the global stiffness and mass matrices does not increase the determinant size of the final eigenvalue equation.

2.5. Shape functions for selected case studies

2.5.1. Simply supported square plate with centrally located discontinuity ($a/b = 1.0$; $c/a = 0.4$; $D_I = 4D$; $D_{II} = D$; $v = 0$)

Suitable boundary conditions are imposed along the axis symmetric edges to obtain the symmetry and anti-symmetry modes of the simply supported plate under consideration here. The symmetry modes are obtained by enforcing zero slope and zero shear force at the symmetry edge, while anti-symmetry modes are obtained from the boundary conditions of zero displacement and zero moment. The admissible functions

used for the plate deflection functions are derived from the boundary conditions associated with each subdomain.

(i) *Doubly symmetry modes:* The boundary conditions associated with the doubly symmetric (SS) modes of the fully supported square plate are simply supported-symmetry along both x and y directions for all four subdomains. The x and y ranges for all subdomains are $(0 \leqslant x \leqslant a)$ and $(0 \leqslant y \leqslant b)$ respectively. Hence, the basic and generating functions for the SS modes of a simply supported square plate with a centrally located sectional discontinuity are

$$\phi_1^{\{\varepsilon\}}(x) = 8x - 4x^3 + x^4, \qquad g^{\{\varepsilon\}}(x) = -2 + x^2, \quad \varepsilon = 1,2,3,4 \tag{39a}$$

$$\psi_1^{\{\varepsilon\}}(y) = 8y - 4y^3 + y^4, \qquad g^{\{\varepsilon\}}(y) = -2 + y^2, \quad \varepsilon = 1,2,3,4 \tag{39b}$$

(ii) *Doubly antisymmetry modes:* The boundary conditions associated with the doubly antisymmetric (AA) modes of the fully supported square plate are simply supported–simply supported along both x and y directions for all domains. The x and y ranges for all subdomains remain unchanged at $(0 \leqslant x \leqslant a)$ and $(0 \leqslant y \leqslant b)$ respectively. Hence, the basic and generating functions for the AA modes may be expressed as follows

$$\phi_1^{\{\varepsilon\}}(x) = x - 2x^3 + x^4, \qquad g^{\{\varepsilon\}}(x) = x^2, \quad \varepsilon = 1,2,3,4 \tag{40a}$$

$$\psi_1^{\{\varepsilon\}}(y) = y - 2y^3 + y^4, \qquad g^{\{\varepsilon\}}(y) = y^2, \quad \varepsilon = 1,2,3,4 \tag{40b}$$

(iii) *Antisymmetry–symmetry modes:* The boundary conditions associated with the antisymmetric-symmetry (AS) modes of the fully supported square plate are simply supported–simply supported along the x direction and simply supported-symmetry along the y direction for all four domains. The x and y ranges for all subdomains remain unchanged again at $(0 \leqslant x \leqslant a)$ and $(0 \leqslant y \leqslant b)$ respectively. Thus, the basic and generating functions for the AS modes can be obtained as

$$\phi_1^{\{\varepsilon\}}(x) = x - 2x^3 + x^4, \qquad g^{\{\varepsilon\}}(x) = x^2, \quad \varepsilon = 1,2,3,4 \tag{41a}$$

$$\psi_1^{\{\varepsilon\}}(y) = 8y - 4y^3 + y^4, \qquad g^{\{\varepsilon\}}(y) = -2 + y^2, \quad \varepsilon = 1,2,3,4 \tag{41b}$$

(iv) *Symmetry–antisymmetry modes:* The boundary conditions associated with the symmetry-antisymmetric (SA) modes of the fully supported square plate are the exact opposite to those from the AS mode of analysis, being; simply supported-symmetry along the x direction and simply supported–simply supported along the y direction for all subdomains. The x and y ranges for all subdomains remain unchanged at $(0 \leqslant x \leqslant a)$ and $(0 \leqslant y \leqslant b)$ respectively. Hence, the basic and generating functions for the SA mode of analysis are

$$\phi_1^{\{\varepsilon\}}(x) = 8x - 4x^3 + x^4, \qquad g^{\{\varepsilon\}}(x) = -2x + x^2, \quad \varepsilon = 1,2,3,4 \tag{42a}$$

$$\psi_1^{\{\varepsilon\}}(y) = y - 2y^3 + y^4, \qquad g^{\{\varepsilon\}}(y) = y^2, \quad \varepsilon = 1,2,3,4 \tag{42b}$$

2.5.2. Clamped–simply supported–clamped–simply supported square plate with centrally located discontinuity ($a/b = 1.0$; $c/a = 0.4$; $D_I = 4D$; $D_{II} = D$; $v = 0$)

The boundary conditions of the basic square element for a CSCS plate are consistent for all the subdomains in both the x and y directions and are associated to the types of modes being considered. Thus, for the SS modes of a CSCS square plate, the boundary conditions are clamped-symmetry along the x direction and simply supported-symmetry along the y direction for all four subdomains. For AA modes, the

associated boundary conditions are clamped-simply supported along the x direction and simply supported–simply supported along the y direction for all subdomains.

Similarly, the boundary conditions associated with the AS modes of the CSCS square plate are clamped–simply supported along the x direction and simply supported-symmetry along the y direction for all four subdomains. In the same manner, the boundary conditions associated with SA modes of the CSCS square plate can be taken as simply supported-symmetry along the x direction and simply supported–simply supported along the y direction for all subdomains.

The basic generating functions for the various types of mode analysis are derived from the associated boundary conditions of the basic square element for a CSCS plate. The x and y ranges are consistent at $(0 \leqslant x \leqslant a)$ and $(0 \leqslant y \leqslant b)$ respectively for all four subdomains. Thus, the basic and generating functions derived for each type of mode analysis may be expressed as follows:

(i) *Doubly symmetry modes*

$$\phi_1^{\{\varepsilon\}}(x) = 4x^2 - 4x^3 + x^4, \qquad g^{\{\varepsilon\}}(x) = -2x + x^2, \quad \varepsilon = 1,2,3,4 \tag{43a}$$

$$\psi_1^{\{\varepsilon\}}(y) = 8y - 4y^3 + y^4, \qquad g^{\{\varepsilon\}}(y) = -2 + y^2, \quad \varepsilon = 1,2,3,4 \tag{43b}$$

(ii) *Doubly antisymmetry modes*

$$\phi_1^{\{\varepsilon\}}(x) = 3x^2 - 5x^3 + x^4, \qquad g^{\{\varepsilon\}}(x) = x, \quad \varepsilon = 1,2,3,4 \tag{44a}$$

$$\psi_1^{\{\varepsilon\}}(y) = y - 2y^3 + y^4, \qquad g^{\{\varepsilon\}}(y) = y^2, \quad \varepsilon = 1,2,3,4 \tag{44b}$$

(iii) *Antisymmetry–symmetry modes*

$$\phi_1^{\{\varepsilon\}}(x) = 3x^2 - 5x^3 + x^4, \qquad g^{\{\varepsilon\}}(x) = x, \quad \varepsilon = 1,2,3,4 \tag{45a}$$

$$\psi_1^{\{\varepsilon\}}(y) = 8y - 4y^3 + y^4, \qquad g^{\{\varepsilon\}}(y) = -2y + y^2, \quad \varepsilon = 1,2,3,4 \tag{45b}$$

(iv) *Symmetry–antisymmetry modes*

$$\phi_1^{\{\varepsilon\}}(x) = 4x^2 - 4x^3 + x^4, \qquad g^{\{\varepsilon\}}(x) = -2x + x^2, \quad \varepsilon = 1,2,3,4 \tag{46a}$$

$$\psi_1^{\{\varepsilon\}}(y) = y - 2y^3 + y^4, \qquad g^{\{\varepsilon\}}(y) = y^2, \quad \varepsilon = 1,2,3,4 \tag{46b}$$

2.5.3. Fully clamped square plate with centrally located discontinuity ($a/b = 1.0$; $c/a = 0.4$; $d_i = 4d$; $d_{ii} = d$; $v = 0.0$)

The boundary conditions of the basic square element for a fully clamped plate are similar for all the subdomains in both the x and y directions and are associated according to the types of mode analysis being considered. Hence, for the SS modes of the fully clamped plate, the boundary conditions are clamped-symmetry along both the x and y directions for all four subdomains. For the AA modes, the associated boundary conditions are clamped–simply supported along both the x and y directions for all subdomains.

Similarly, the boundary conditions associated with the AS modes of the fully clamped square plate are clamped-simply supported along the x direction and clamped-symmetry along the y direction for all four subdomains. In the same manner, the boundary conditions associated with SA modes of the fully clamped square plate can be taken as clamped-symmetry along the x direction and clamped-simply supported along the y direction.

As in the previous case, the basic and generating functions for various types of mode analysis are derived from the associated boundary conditions of the basic square element for a fully clamped plate. The x and y

ranges are consistent at $(0 \leqslant x \leqslant a)$ and $(0 \leqslant y \leqslant b)$ respectively for all four subdomains. Thus, the basic and generating functions for each type of mode analysis may be derived as follows:

(i) *Doubly symmetry modes*

$$\phi_1^{\{\varepsilon\}}(x) = 4x^2 - 4x^3 + x^4, \qquad g^{\{\varepsilon\}}(x) = -2x + x^2, \quad \varepsilon = 1,2,3,4 \tag{47a}$$

$$\psi_1^{\{\varepsilon\}}(y) = 4y^2 - 4y^3 + y^4, \qquad g^{\{\varepsilon\}}(y) = -2y + y^2, \quad \varepsilon = 1,2,3,4 \tag{47b}$$

(ii) *Doubly antisymmetry modes*

$$\phi_1^{\{\varepsilon\}}(x) = 3x^2 - 5x^3 + x^4, \qquad g^{\{\varepsilon\}}(x) = x, \quad \varepsilon = 1,2,3,4 \tag{48a}$$

$$\psi_1^{\{\varepsilon\}}(y) = 3y^2 - 5y^3 + y^4, \qquad g^{\{\varepsilon\}}(y) = y, \quad \varepsilon = 1,2,3,4 \tag{48b}$$

(iii) *Antisymmetry–symmetry modes*

$$\phi_1^{\{\varepsilon\}}(x) = 3x^2 - 5x^3 + x^4, \qquad g^{\{\varepsilon\}}(x) = x, \quad \varepsilon = 1,2,3,4 \tag{49a}$$

$$\psi_1^{\{\varepsilon\}}(y) = 4y^2 - 4y^3 + y^4, \qquad g^{\{\varepsilon\}}(y) = -2y + y^2, \quad \varepsilon = 1,2,3,4 \tag{49b}$$

(iv) *Symmetry–antisymmetry modes*

$$\phi_1^{\{\varepsilon\}}(x) = 4x - 4x^3 + x^4, \qquad g^{\{\varepsilon\}}(x) = -2x + x^2, \quad \varepsilon = 1,2,3,4 \tag{50a}$$

$$\psi_1^{\{\varepsilon\}}(y) = 3y^2 - 5y^3 + y^4, \qquad g^{\{\varepsilon\}}(y) = y, \quad \varepsilon = 1,2,3,4 \tag{50b}$$

3. Results and discussion

The convergence study for the simply supported square plate is tabulated in Table 1. The study shows a monotonically downward convergence at 9×9 terms for the SS modes and at 10×10 terms for the AA modes. The results in Table 2 compare well with those reported by Tham et al. (1986) in which a negative stiffness approach was used. Very good agreement is also observed when compared with the results reported by Lam et al. (1989). A maximum deviation of less than 0.5% is observed for the simply supported case and a maximum deviation of less than 1.2% for the first few modes of the fully clamped case. Excellent agreement was also obtained against the finite difference results of Aksu and Ali (1976).

Parametric studies have been performed for both simply supported and fully clamped square plates with abrupt cross section. The result for the first symmetry (SS) mode follows closely to those reported by Lam et al. (1989). A wide range of new parametric curves is illustrated in Figs. 2 and 3 for the simply supported and fully clamped square plates respectively.

The mode shapes for the simply supported square plate with the centrally located cross-sectional discontinuity are illustrated in Fig. 4 in the form of contour plots. Corresponding results for the CSCS and fully clamped square plates are presented in Figs. 5 and 6 respectively. It is observed that the mode shapes for both the fully clamped and simply supported plates are quite similar. This similarity is due to the symmetrical nature of their configurations. The mode shapes for the CSCS plate, however, are significantly different due to the presence of only one symmetry axis and this is clearly evident from the figures.

Table 1
Convergence of frequency parameter, $\lambda = \omega a^2(\rho h/D)^{1/2}$, of a simply supported square plate with centrally located abrupt section ($a/b = 1.0; c/a = 0.4; \gamma = 0.6; D_{\mathrm{I}} = 4D; D_{\mathrm{II}} = D; \nu = 0.0$)

Terms $I \times J$	Segments Mq	Mode sequence number					
		1	2	3	4	5	6
(a) SS mode							
4×4	4	30.54	148.3	153.1	267.5	423.3	423.4
5×5	5	30.51	147.5	151.2	263.9	384.8	387.4
6×6	6	30.50	146.8	149.9	261.5	369.9	374.4
7×7	7	30.47	146.5	149.4	260.4	361.0	366.4
8×8	8	30.44	146.4	149.3	260.2	357.9	363.1
9×9	9	30.44	146.4	149.2	260.1	357.7	362.6
(b) SA mode							
4×4	4	73.95	193.3	242.3	373.4	468.0	529.3
5×5	5	73.75	192.3	242.0	370.5	440.4	523.9
6×6	6	73.62	191.8	241.4	368.4	434.8	523.6
7×7	7	73.42	191.6	241.4	367.7	432.2	518.9
8×8	8	73.40	191.6	241.2	367.5	431.3	518.6
9×9	9	73.27	191.5	241.0	367.4	431.2	516.3
10×10	10	73.26	191.4	241.0	367.4	431.2	515.5
(c) AS mode							
4×4	4	73.95	193.3	242.3	373.4	468.0	529.3
5×5	5	73.75	192.3	242.0	370.5	440.4	523.9
6×6	6	73.62	191.8	241.4	368.4	434.8	523.6
7×7	7	73.42	191.6	241.4	367.7	432.2	523.9
8×8	8	73.40	191.6	241.2	367.5	431.3	518.6
9×9	9	73.27	191.5	241.0	367.4	431.2	518.3
10×10	10	73.26	191.4	241.0	367.4	431.2	515.5
(d) AA mode							
4×4	4	117.4	296.2	301.6	477.7	607.4	608.8
5×5	5	117.3	296.2	301.4	476.5	595.7	597.0
6×6	6	117.2	295.5	301.3	475.1	595.2	596.7
7×7	7	117.1	295.5	301.3	474.9	593.6	595.2
8×8	8	117.1	295.3	301.2	474.2	593.4	594.9
9×9	9	117.0	295.2	301.2	474.2	592.3	594.2
10×10	10	117.0	295.2	301.2	474.0	592.3	593.7

Table 2
Comparison of frequency parameter, $\lambda = \omega a^2(\rho h/D)^{1/2}$, for square plates with centrally located square abrupt cross section ($a/b = 1.0; D_{\mathrm{I}} = 4D; D_{\mathrm{II}} = D; \nu = 0$)

Inner side ratio c/a	Finite difference Aksu and Ali (1976)	Modified R–R Lam et al. (1989)	Negative stiffness Tham et al. (1986)	Present method
(a) Simply supported square plate				
0.00	31.14	31.34	31.34	31.33
0.25	30.46	31.04	30.90	30.87
0.50	29.58	30.18	30.22	30.11
0.75	26.74	27.65	27.61	27.63
1.00	19.52	19.74	19.74	19.74
(b) Fully clamped square plate				
0.00	–	57.15	57.07	57.12
0.25	–	57.46	57.28	57.29
0.50	56.14	58.40	58.50	58.27
0.75	–	51.22	52.11	50.49
1.00	34.85	35.99	35.98	35.98

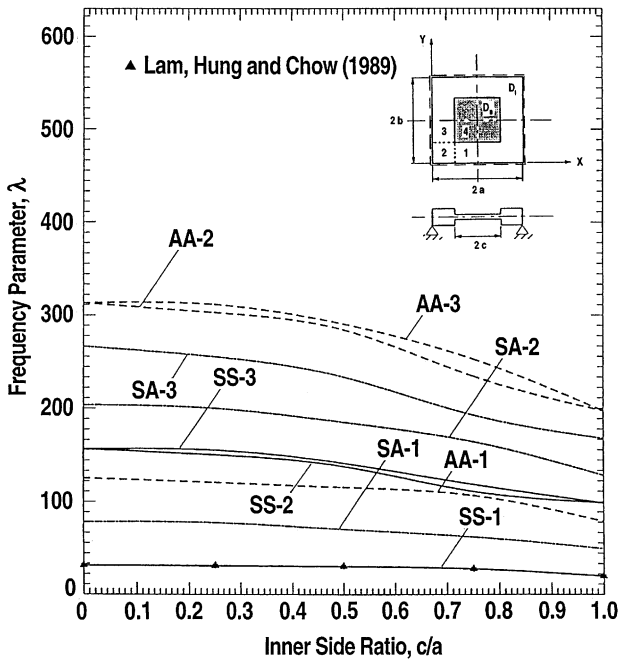

Fig. 2. Parametric study of a simply supported square plate with a centrally located abrupt cross section ($a/b = 1.0; c/a = 0.4; D_{\mathrm{I}} = 4D; D_{\mathrm{II}} = D; v = 0.0$); 'Δ' as defined in Lam et al. (1989).

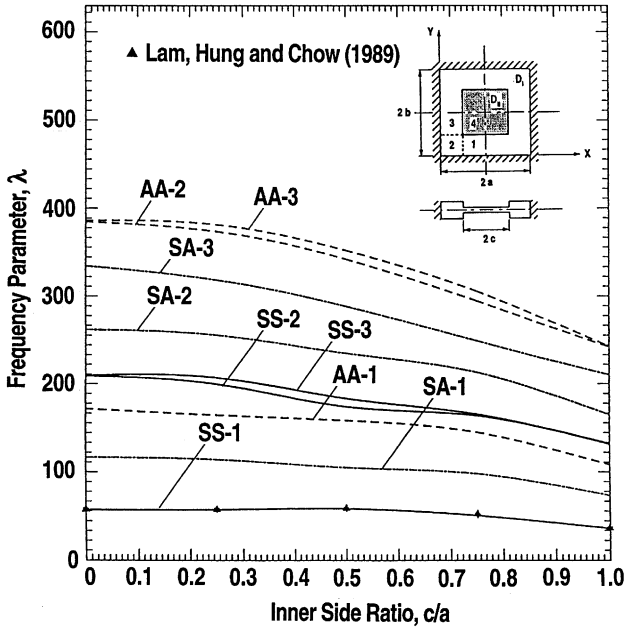

Fig. 3. Parametric study of a fully clamped square plate with a centrally located abrupt cross section ($a/b = 1.0; c/a = 0.4; D_{\mathrm{I}} = 4D; D_{\mathrm{II}} = D; v = 0.0$); 'Δ' as defined in Lam et al. (1989).

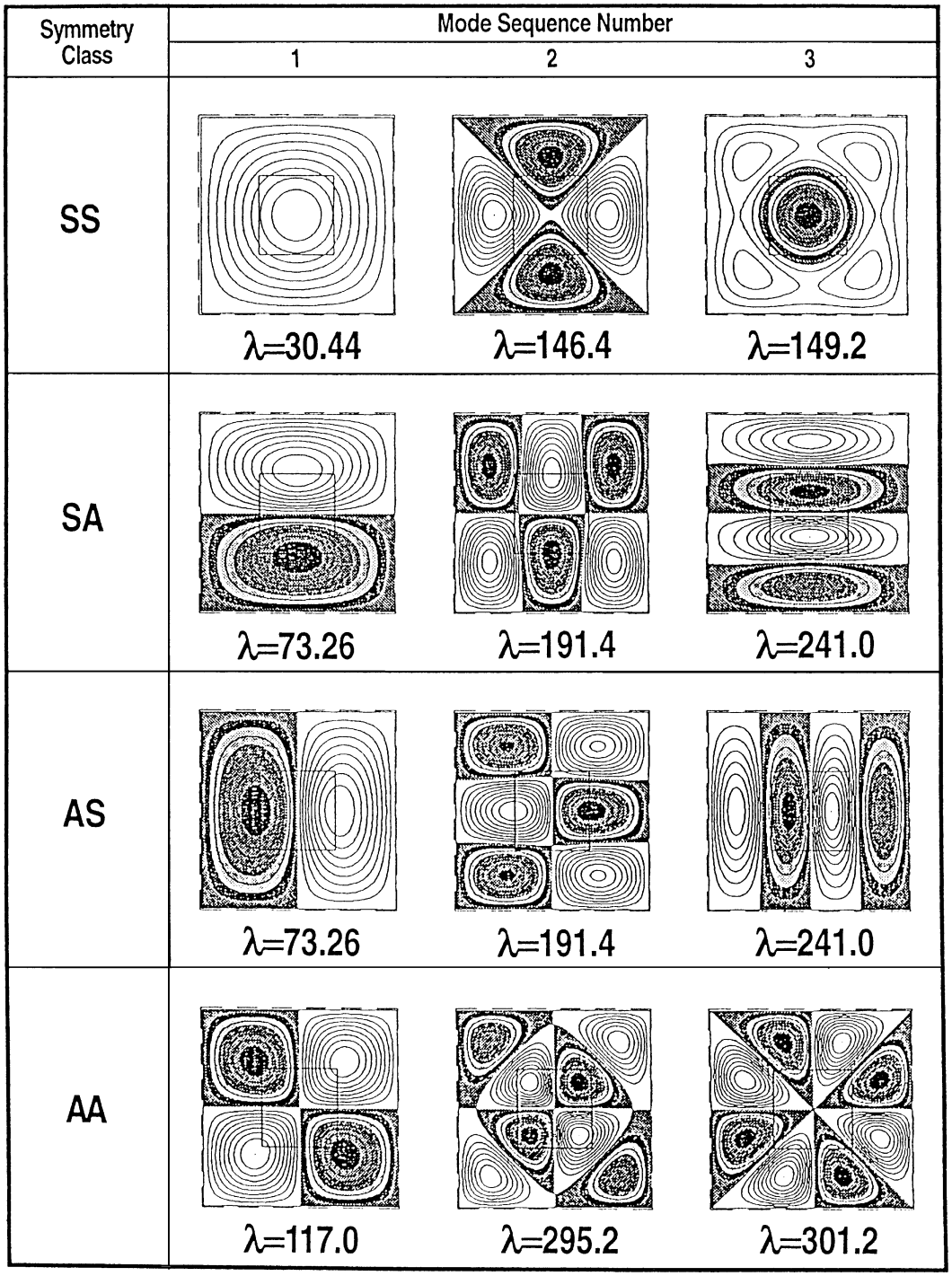

Fig. 4. Contour plots of deflection mode shapes for a simply supported square plate with a centrally located abrupt cross section ($a/b = 1.0; c/a = 0.4; D_{\mathrm{I}} = 4D; D_{\mathrm{II}} = D; v = 0.0$).

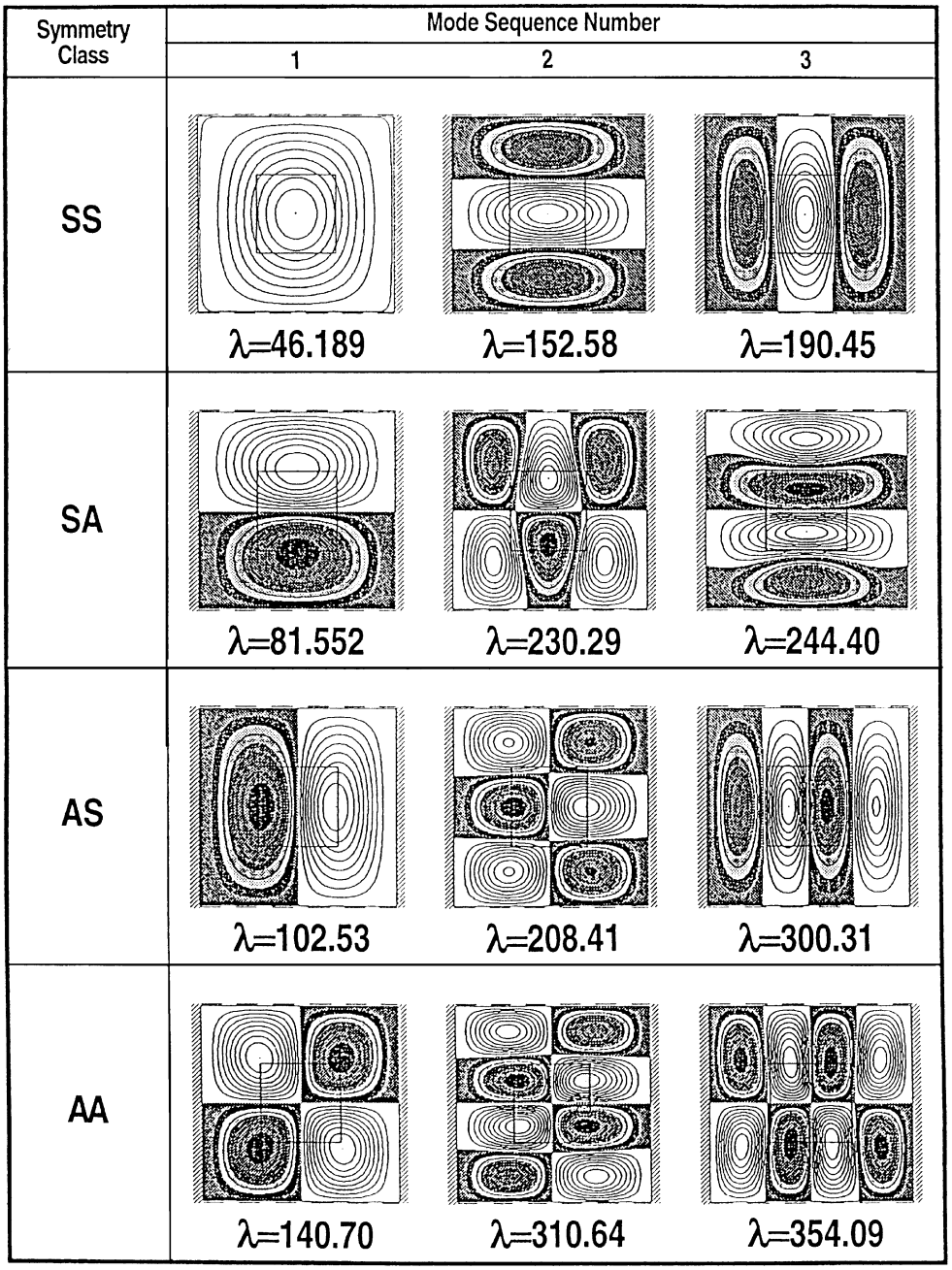

Fig. 5. Contour plots of deflection mode shapes for a CSCS square plate with a centrally located abrupt cross section ($a/b = 1.0; c/a = 0.4; D_{\mathrm{I}} = 4D; D_{\mathrm{II}} = D; \nu = 0.0$).

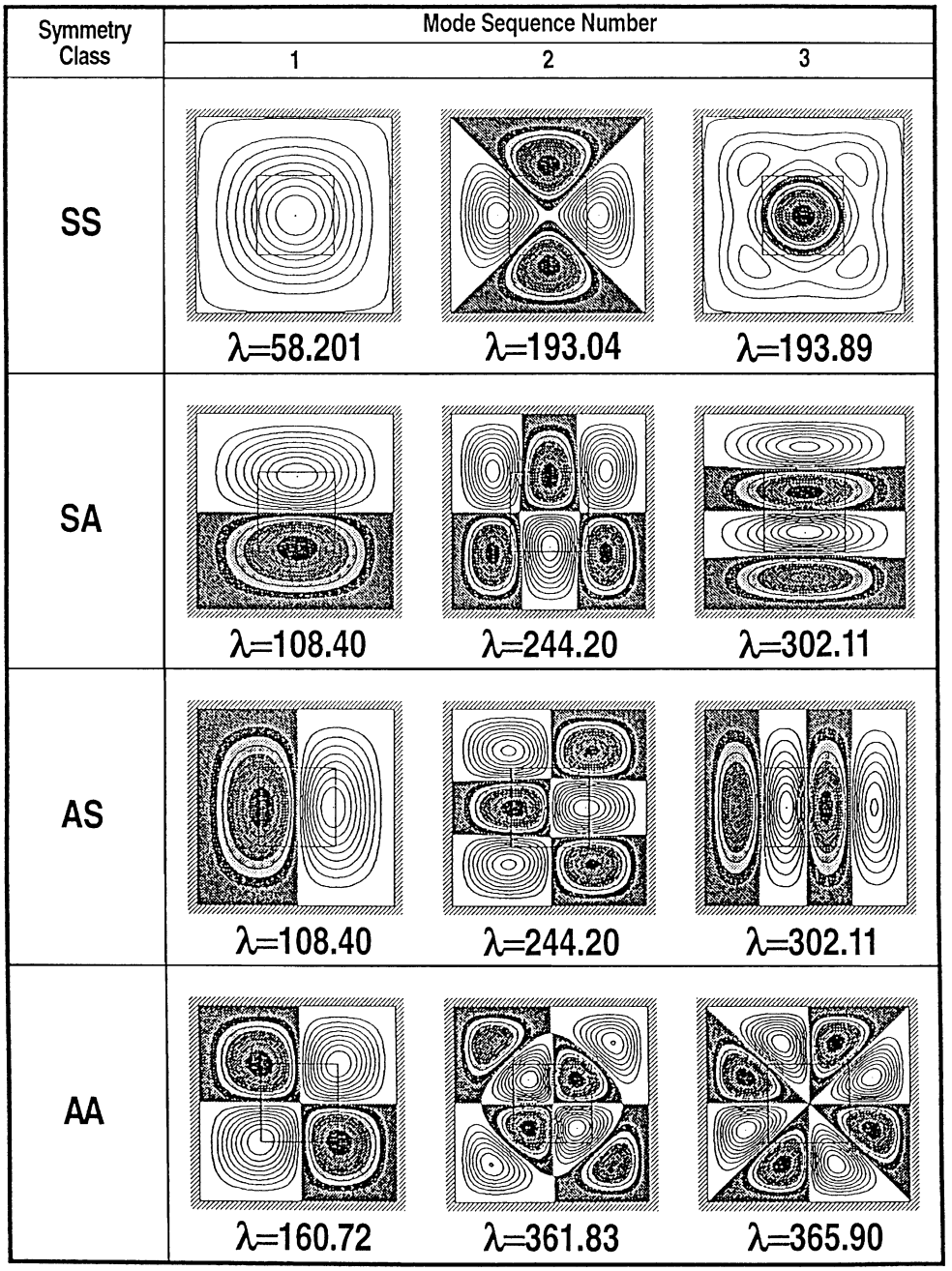

Fig. 6. Contour plots of deflection mode shapes for a fully clamped square plate with a centrally located abrupt cross section ($a/b = 1.0; c/a = 0.4; D_{\mathrm{I}} = 4D; D_{\mathrm{II}} = D; \nu = 0.0$).

4. Conclusions

A semi-analytical technique based on the domain decomposition method has been presented for the vibration analysis of thin isotropic plates with cross sectional discontinuities in the form of abrupt changes in thickness. The flexibility and computational efficiency of the methodology has been demonstrated by considering square plates with centrally located discontinuities and for three boundary condition types. From comparisons with results available in the literature, the accuracy of the method has been validated as very good agreements was established. The computed natural frequencies have been documented in tabular form and the contour plots of a range of new mode shapes have been presented. This work has been restricted to thin plates. An extension for possible future work is to include the effects of shear deformation and rotary inertia so as to cater for thick plates with abrupt thickness changes.

References

Aksu, G., Ali, R., 1976. Determination of dynamic characteristics of rectangular plates with cut-outs using finite difference formulation. Journal of Sound and Vibration 44, 147–158.

Boay, C.G., 1996. Free vibration of laminated plates with a central circular hole. Composite Structures 35, 357–368.

Chau, K.T., Wang, Y.B., 1999. A new boundary integral formulation for plane elastic bodies containing cracks and holes. International Journal of Solids and Structures 36, 2041–2074.

Chihara, T.S., 1978. An Introduction to Orthogonal Polynomials. Gordon and Breach, New York.

Geannakakes, G.N., 1990. Vibration analysis of arbitrarily shaped plates using beam characteristic orthogonal polynomials in the semi-analytical finite strip method. Journal of Sound and Vibration 137, 283–303.

Grandin Jr., H., 1986. Fundamentals of the Finite Element Method. Macmillan, New York.

Lam, K.Y., Hung, K.C., Chow, S.T., 1989. Vibration analysis of plates with cutouts by the modified Rayleigh–Ritz method. Applied Acoustics 28, 49–60.

Laura, P.A.A., Avalos, D.R., Larrondo, H.A., 1990. Forced vibrations of circular, stepped plates. Journal of Sound and Vibration 136, 146–150.

Laura, P.A.A., Romanelli, E., Rossi, R.E., 1997. Transverse vibrations of simply supported rectangular plates with rectangular cutouts. Journal of Sound and Vibration 202, 275–283.

Liew, K.M., Hung, K.C., Lim, M.K., 1993a. Method of domain decomposition in vibrations of mixed edge anisotropic plates. International Journal of Solids and Structures 30, 3281–3301.

Liew, K.M., Hung, K.C., Lim, M.K., 1993b. Roles of domain decomposition method in plate vibrations - treatment of mixed discontinuous periphery boundaries. International Journal of Mechanical Sciences 35, 615–632.

Liew, K.M., Hung, K.C., Sum, Y.K., 1995. Flexural vibration of polygonal plates: treatments of sharp re-entrant corners. Journal of Sound and Vibration 183, 221–238.

Liew, K.M., Sum, Y.K., 1998. Vibration of plates having orthogonal straight edges with clamped boundaries. Transactions of ASCE Journal of Engineering Mechanics 124, 184–192.

Liu, F.L., Liew, K.M., 1999a. Vibration analysis of discontinuous Mindlin plates by differential quadrature element method. Transaction of ASME Journal of Vibration and Acoustics 121, 204–208.

Liu, F.L., Liew, K.M., 1999b. Differential quadrature element method: a new approach for free vibration analysis of polar Mindlin plates having discontinuities. Computer Methods in Applied Mechanics and Engineering 179, 407–423.

Pan, E.N., 1997. A general boundary element analysis of 2-D linear elastic fracture mechanics. International Journal of Fracture 88, 41–59.

Rao, C.R., Mitra, S.K., 1971. Generalized Inverse of Matrices and Its Applications. Wiley, New York.

Sabir, A.B., Davies, G.T., 1997. Natural frequencies of square plates with reinforced central holes subjected to inplane loads. Thin-Walled Structures 28, 337–353.

Sivakumar, K., Iyengar, N.G.R., Deb, K., 1999a. Free vibration of laminated composite plates with cutout. Journal of Sound and Vibration 221, 443–470.

Sivakumar, K., Iyengar, N.G.R., Deb, K., 1999b. Optimum design of laminated composite plates with cutouts undergoing large amplitude oscillations. Advanced Composite Materials 8, 295–316.

Tham, L.C., Chan, A.H.C., Cheung, Y.K., 1986. Free vibration and buckling analysis of plates by the negative stiffness method. Computers and Structures 22, 687–692.

Yang, B., Park, D.H., 1999. Analysis of plates with curved boundaries using isoparametric strip distributed transfer functions. International Journal for Numerical Methods in Engineering 44, 131–146.

Yang, B., Zhou, J., 1996. Semi-analytical solution of 2-D elasticity problems by the strip distributed transfer function method. International Journal of Solids and Structures 33, 3983–4005.